Published in final edited form as:
J Inorg Biochem. 2009 June ; 103(6): 906–911. doi:10.1016/j.jinorgbio.2009.04.001.

Nanosecond photoreduction of inducible nitric oxide synthase by a Ru-diimine electron tunneling wire bound distant from the active site

Charlotte A. Whited[a], **Wendy Belliston-Bittner**[a], **Alexander R. Dunn**[a,b], **Jay R. Winkler**[*,a], and **Harry B. Gray**[*,a]

a*Beckman Institute, California Institute of Technology, Pasadena, California 91125*

b*Department of Chemical Engineering, Stanford University, Stanford, California 94305*

Abstract

A Ru-diimine wire, $[(4,4',5,5'\text{-tetramethylbipyridine})_2Ru(F_9bp)]^{2+}$ (tmRu-F_9bp, where F_9bp is 4-methyl-4'-methylperfluorobiphenylbipyridine), binds tightly to the oxidase domain of inducible nitric oxide synthase (iNOSoxy). The binding of tmRu-F_9bp is independent of tetrahydrobiopterin, arginine, and imidazole, indicating that the wire resides on the surface of the enzyme, distant from the active-site heme. Photoreduction of an imidazole-bound active-site heme iron in the enzyme-wire conjugate ($k_{ET} = 2(1) \times 10^7\ s^{-1}$) is fully seven orders of magnitude faster than the *in vivo* process.

Introduction

Nitric oxide synthase (NOS) is a heme monooxygenase that catalyzes the five-electron oxidation of L-arginine and O_2 to citrulline and nitric oxide (NO). NOS effects this transformation in two turnovers, producing N^G-hydroxy-L-arginine (NHA) as an enzyme-bound intermediate, requiring three electrons from its reductase domain. Each turnover is expected to proceed through a mechanism similar to that of cytochrome P450 (although the two turnovers may utilize a different species for substrate oxidation), central to which are two slow electron transfer (ET) events [1-6]. The first ET event reduces the resting, substrate-bound heme to the ferrous state, which then binds oxygen to create the last observable intermediate (ferric-superoxo) [4,7]. It is thought that the second ET event, where the electron is supplied by the cofactor tetrahydrobiopterin (BH_4), produces one or more high-valent heme species, with substrate oxidation possibly occurring from a ferryl-porphyrin$^{+\bullet}$ intermediate (Compound I) [4,8]. The sluggishness of the second ET step, however, has so far prevented the characterization of high-valent intermediates in the catalytic cycle in solution [3,4,9]. Cryoreduction of the heme domain of ferric-superoxo endothelial NOS at 77 K leads to the formation of a ferric-peroxo species [3]. Annealing at 165 K results in conversion to the product state without the appearance of intermediates. These data suggest that O-O bond cleavage is slower than reaction with substrate.

By employing laser-induced ET to reduce the active-site heme very rapidly, it should be possible to observe high-valent intermediates that follow in the catalytic cycle. Toward this

*Corresponding author. Email: E-mail: winklerj@caltech.edu, E-mail: hbgray@caltech.edu.

end, we and others have developed photoactive electron tunneling wires to deliver electrons and holes to and from the deeply buried heme active sites in P450cam [10-12] and NOS [13-16]. Importantly, one of the NOS wires, tmRu-F_9bp (Chart 1), can potentially probe the catalytic cycle, since it binds tightly and specifically to the oxidase domain of the inducible form of the enzyme (iNOSoxy) in a region that is *distant* from the active site [17]. Here we demonstrate that an imidazole-ligated heme in tmRu-F_9bp:iNOSoxy can be photoreduced several million times faster (k_{ET} = 2(1) × 10^7 s^{-1}) than the physiological ET reaction.

Materials and Methods

General

The tmRu-F_9bp complex was synthesized as described previously [11,18,19]. Tetramethylphenylenediamine (TMPD) was obtained from Aldrich and vacuum-sublimed before use. BH_4 (Aldrich) was stored under argon at -20 °C. All other chemicals were used as received from Sigma, JT Baker, Fischer, EM Sciences, and Mallinckrodt. UV-visible absorption spectra were acquired on an Agilent 8453 UV spectrometer. Gel electrophoresis was run on a Phast System (Pharmacia) with 8-25 percent gradient precast agarose gels and SDS buffer strips. Samples were loaded in 4x SDS buffer and stained with Coomassie blue. Samples were run against Precision Plus All-Blue standards (BioRad).

iNOSoxy expression and purification

The heme domain of iNOS with a C-terminal His_6 tag was overexpressed in *E. coli* and purified as described previously [20] with several exceptions. Briefly, expression cells were subjected to two rounds of chemical lysis by pelleting and resuspension in 40 mL of B-PER lysis buffer (protein extraction reagent B, Pierce). The lysis buffer included a cocktail of protease inhibitors (10 μg/mL benzamidine, 5 μg/mL leupeptin, 1 μg/mL each pepstatin, antipain, and chymostatin, and ~500 μM Pefabloc (Roche)) as well as 100 μg/mL DNase, 100 μg/mL RNase, ~500 μg/mL lysozyme, and 20 mM imidazole per liter of cells. The suspension was centrifuged and the supernatant was loaded directly onto a His_6 immobilized metalion affinity chromatography column (5 mL Ni^{2+}:HisTrap, Amersham). Once the protein was completely loaded, it was washed with 20 column volumes of 20 mM imidazole in 50 mM NaP_i/300 mM NaCl/pH 8. The protein was eluted with 150 mM imidazole and concentrated to ~3 mL in an Amicon Ultra centrifugation device (10,000 MWCO, Millipore). The concentrated sample was then further purified over a size-exclusion column, as described previously [20]. The anion exchange column was omitted when ≥95 percent purity was confirmed by UV-visible spectroscopy and gel electrophoresis. The purified protein was concentrated to ~200 μM, divided into 100 μL aliquots, and stored in 50 percent glycerol at -80 °C.

Sample preparation

Small aliquots of iNOSoxy were thawed and exchanged into phosphate buffer (50 mM KP_i, 50 mM KCl, pH 7.4) using a PD-10 desalting column (BioRad) immediately before use. The position of the heme Soret maximum (422 nm) confirmed the presence of low-spin, water-bound heme [17,20]. The heme protein concentration was determined using ε_{422} = 75 $mM^{-1}cm^{-1}$ per unit heme [17]. For the inhibitor-bound samples, imidazole (400-500 μM) was added, and binding was confirmed by a Soret shift to 428 nm [17,20]. For substrate-bound, pterin-free samples, 1 mM arginine was added to dilute (~2-20 μM) iNOSoxy and allowed to incubate at 4 °C for approximately 30 min. In the absence of pterin (BH_4), only partial conversion to a high-spin heme (λ_{max} = 398 nm [20,21]) was observed. For substrate- and pterin-bound samples, fresh BH_4 solutions were prepared daily. Phosphate buffer was thoroughly deoxygenated by bubbling with argon for ≥10 min. Solid BH_4 was added to the degassed buffer under a counter-flow of argon. Dilute iNOSoxy (~2-20 μM) was deoxygenated by at least 30 evacuation-Ar backfill cycles, taking care to avoid bubbling of the solution.

Aliquots of concentrated, deoxygenated pterin and arginine stocks were then added to the protein solution, giving final concentrations of 100 μM BH_4 and 1 mM arginine. The solution was incubated for 2 h at 4 °C; binding of BH_4 and arginine was confirmed by a Soret shift to 396 nm [22,23].

For quenching experiments, 1 M ascorbate stock solutions were prepared daily by dissolving ascorbate in thoroughly deoxygenated 1 M KOH. Ascorbate (1 M) and solid TMPD were added to deoxygenated protein solutions under a counter-flow of argon.

Transient spectroscopy

Luminescence decay and transient absorption measurements were made as described previously [24-26]. The ~8 ns, 480 nm excitation pulses were produced by a Nd:YAG pumped optical parametric oscillator. Data were collected at 1×10^9 samples s^{-1} using a LeCroy digital oscilloscope. Transient absorbance data were converted from intensity to absorbance using the following expression (Eq. 1):

$$\Delta Abs = -\log\left(\frac{I}{I_0}\right) \tag{1}$$

where I is the intensity of light transmitted through the sample excitation volume, and I_0 is the average transmitted light intensity during the 200 ns prior to the laser shot. Luminescence decay curves and transient absorbance traces were fit to one, two, or three exponentials using a nonlinear least-squares algorithm (Eq. 2, Igor Pro):

$$I(t) = c_0 + \sum_n c_n e^{-k_n t} \tag{2}$$

Each experiment was repeated at least three times unless indicated otherwise.

Determination of $Ru^{I}\rightarrow Fe^{III}$ ET rate constants

At a given time after excitation, the absorbance observed at a given wavelength (λ) between 400 and 450 nm is (Eq. 3):

$$\Delta Abs = \left(\varepsilon_{Fe^{II}} - \varepsilon_{Fe^{III}}\right)\left[Fe^{II}\right] + \left(\varepsilon_{*Ru^{II}} - \varepsilon_{Ru^{II}}\right)\left[*Ru^{II}\right] + \left(\varepsilon_{Ru^{I}} - \varepsilon_{Ru^{II}}\right)\left[Ru^{I}\right] \tag{3}$$

Since ascorbate, TMPD, and $TMPD^{+\bullet}$ do not absorb strongly in this region (under the conditions of these experiments, Figure S2), the contributions of these species were neglected. Owing to substantial populations of unbound Ru-complex, the absorbance changes at these wavelengths due to depopulation of Ru^{II} and formation of $*Ru^{II}$ are large compared to those for Fe^{II} formation because $[*Ru^{II}] \gg [Fe^{II}]$. Moreover, the presence of both free and iNOSoxy-bound wire complicates the transient absorbance kinetics. In fitting these data, we were unable to identify a phase that was distinct from those corresponding to $*Ru^{II}$ decay in bound and free wires, and that reliably could be attributed to intraprotein ET from Ru^{I} to Fe^{III} (k_{ET}).

In order to characterize the Ru^{I} to Fe^{III} ET kinetics, we developed a procedure to remove the $*Ru^{II}$ contribution from the transient absorbance kinetics. The isosbestic point for low-spin, imidazole-bound Fe^{III} iNOSoxy and the product Fe^{II} species occurs at 438 nm. In each

experiment, therefore, transient absorbance of the Im-iNOSoxy/wire/quencher system at 438 nm reflects the $*Ru^{II}$ bleach and recovery, but contains no contribution from iNOSoxy. Using an experimentally validated $*Ru^{II}$-Ru^{II} difference spectrum, we determined scaling factors by which we could multiply the 438 nm transient signals to produce estimates of the $*Ru^{II}$ contributions to the observed kinetics at several other wavelengths ([$*Ru^{II}$-Ru^{II}]: $\Delta\varepsilon_{452}/\Delta\varepsilon_{438} = 1.12$, $\Delta\varepsilon_{425}/\Delta\varepsilon_{438} = 0.66$). The calculated $*Ru^{II}$ signals were subtracted from the observed transient kinetics to produce signals corresponding to the time dependence of [Fe^{II}]. Transient Ru^{I} absorbance was neglected because its $\Delta\varepsilon$ values are <10 percent of those for [Fe^{II}-Fe^{III}] (Figure S5). The resulting corrected traces were then fit to single exponential functions according to Eq. 2.

Results and Discussion

Binding of tmRu-F_9bp to iNOSoxy

We have previously shown that tmRu-F_9bp (Chart 1) binds to iNOSoxy independently of substrate and BH_4 with a dissociation constant of ~1 μM [17]. Remarkably, this wire binds at a site distant from the active-site channel, as demonstrated by the finding that a known channel-binding wire does not displace tmRu-F_9bp from the enzyme [17]. While the precise binding site has not been definitively established, Förster energy transfer measurements indicate that it may be in the hydrophobic pocket thought to be the docking site for the iNOS reductase domain [17,27]. Experiments with $Ru(bpy)_3^{2+}$ show that the photosensitizer alone does not bind to the enzyme (Figure S1), suggesting that the perfluorobiphenyl unit is largely responsible for the strong association of the wire with a hydrophobic iNOSoxy surface region.

Quenching of the bound Ru-wire

In previous work, we described Ru-diimine wires that reduce the heme of cytochrome P450 directly upon photoexcitation [11]. In these experiments the wire termini ligated the iron center, providing an efficient through-bond coupling pathway between the sensitizer and the heme. In contrast, the Ru-wire described here does not directly photoreduce the heme, so we employed a flash/quench method with exogenous reductants to produce Fe^{II} [28]. In this experiment, a quencher (Q) reduces the photoexcited sensitizer to create a strongly reducing species (Ru^{I} in Scheme 1). In the absence of other electron acceptors, the lifetime of Ru^{I} is dependent on the rate of recombination with the oxidized quencher (k_r in Scheme 1). Because Q^+ and Ru^{I} are present at low and equal concentrations, recombination is slow (ms timescale) and heme reduction competes effectively.

Owing to its high solubility in water and lack of spectral interference with heme Soret changes, ascorbate (Asc) is an attractive choice as a quencher for this system. Even at high concentrations (10 mM), however, Asc quenching produces only small yields of Fe^{II} (Figures 1 and 2). TMPD (Figure S3) is a better quencher than Asc, but has limited solubility in water [29, 30]. Further, TMPD autoxidizes to create a soluble bright blue cation radical in aqueous media [31]. Under conditions necessary for efficient excited-state quenching, the production of the radical rapidly turns the solution dark blue, obscuring small transient changes in the heme spectrum (Supporting Information).

These problems were overcome by employing both quenchers [32,33]. In a sample containing 10 mM Asc with saturated TMPD, the superior quenching capability of TMPD can be exploited (Figure 1, red dotted trace) while Asc serves to keep the TMPD reduced. With Asc present, $TMPD^{+\bullet}$ does not accumulate, even after 60 min of photoexcitation in the presence of tmRu-F_9bp.

Rapid production of reduced iNOSoxy

Single wavelength transient absorbance measurements with imidazole-bound iNOSoxy in the presence of one equivalent of tmRu-F_9bp, 10 mM Asc, and saturated TMPD reveal that photochemically generated Ru^I disappears with concomitant formation of a new Fe species within 50 ns of excitation at 480 nm (Figure 3). A difference spectrum constructed from the single-wavelength data at 2 μs (Figure 4) shows the bleach of the Im-Fe^{III} Soret absorption at 428 nm and increased absorbance to the red with a difference-spectrum maximum at 445 nm. The rate of decay of Ru^I and reappearance of Ru^{II} is approximately equal to the rate of changes in the Soret region. Given that Ru^{II} is reformed, the most likely explanation for spectral changes between 400 and 450 nm is Ru^I to Fe^{III} ET, which produces a new Fe^{II} heme species. Control experiments with $Ru(bpy)_3^{2+}$ indicate that the tmRu-F_9bp perfluorobiphenyl moiety is required for heme reduction. In the presence of $Ru(bpy)_3^{2+}$ and quenchers, transient absorbance traces show only the production of Ru^I (Figure S4).

In order to estimate the specific rate of Fe^{II} formation, $*Ru^{II}$ contributions were subtracted from the transient absorbance data as described in Materials and Methods (representative single-wavelength traces are shown in Figure 5). The traces (a minimum of four wavelengths from each of four different experiments completed on different days) were fit to a single exponential function: $k_{ET} = 2(1)\times10^7\ s^{-1}$.

This is a remarkably rapid reduction given the estimated Ru-heme distance of 20.2 Å [17] and the absence of a through-bond pathway to the heme. Given its slim profile, hydrophobicity, and potential to π-stack with aromatic residues, the perfluorobiphenyl moiety of tmRu-F_9bp may intercalate into the protein interior, leaving open the possibility of a through-wire hopping mechanism [13].

Identity of the reduced species

In order to determine the nature of the product of electron transfer to the heme, the six-coordinate Fe^{III}-Im species was reduced under equilibrium conditions for comparison with the transient data. Reaction of Fe^{III}-Im with sodium dithionite in a glove box under an inert atmosphere, followed by removal of excess dithionite on a size-exclusion (PD-10) column equilibrated with 10 mM imidazole, produced a species with the absorption spectrum shown in Figure 6.

Reduction of NOS has been extensively studied [9,23,34-37]. Six-coordinate ferrous-NO and -CO species have been characterized by several investigators [23,36,37]; and, in the absence of arginine and BH_4, it has been shown that these six-coordinate species are unstable. Addition of CO (or NO) to five-coordinate Fe^{II} causes a red-shift in the Soret band to 444 nm (or 440 nm) [23]. The 444 nm band blue-shifts over time to 421 nm, which suggests that a species analogous to the inactive P420 form of cytochrome P450 is produced. It has been proposed that the axial thiolate is not bound to the heme iron in the 421 nm species [23,37].

The blue-shift of the iNOSoxy Soret peak upon dithionite reduction (Figure 6, inset) demonstrates that the red-shifted transient Fe^{II} species produced by photochemical heme reduction likely has different axial coordination. The steady-state Fe^{II} absorption spectrum is in good agreement with that reported for *Drosphila melanogaster* DHR51, a heme protein believed to possess axial Cys and His ligands [38]. Similar spectra have been reported for Fe^{II} forms of mutant cytochrome *c* and myoglobin engineered to have axial Cys and His ligands [39,40]. In each of these Fe^{II} proteins, the Soret maximum is slightly blue-shifted relative to its position in the Fe^{III} form, indicating the presence of a low-spin Fe^{II} heme in which imidazole remains bound but the thiolate ligand has been displaced. Further, five-coordinate ferrous

iNOSoxy has been generated, showing a blue-shift of the Soret from the ferric species similar to the spectrum in Figure 6 [23].

In contrast, the red-shifted Soret band found for photochemically reduced iNOS is analogous to that resulting from cryoreduction of ferric cytochrome P450. Irradiation of six-coordinate low-spin Fe^{III} P450 in a frozen matrix produces a low-spin, presumably six-coordinate Fe^{II} product [41]. Annealing at higher temperatures leads to the high-spin Fe^{II} product that is observed under equilibrium conditions. We suggest that the transient Fe^{II} iNOS species formed by photochemical reduction contains a low-spin Fe^{II} heme with axial Cys and imidazole ligands. In our experiment, this species is likely reoxidized by $TMPD^{+\bullet}$ before loss of axial ligation, which would generate the species observed under equilibrium conditions.

Concluding Remarks

We have developed a system in which the heme of inducible nitric oxide synthase can be photoreduced rapidly without interfering with substrate/cofactor binding. Employing flash-quench experiments with a surface-binding Ru-diimine wire in combination with reductive quenchers, we observed ET to the imidazole-bound heme of iNOSoxy fully seven orders of magnitude faster than the natural reduction. This finding represents an important step toward our goal of identifying reactive intermediates in the catalytic cycles of heme monooxygenases.

Supplementary Material

Refer to Web version on PubMed Central for supplementary material.

Acknowledgments

We thank Michael Marletta for the generous gift of protein reagents and for assistance with the iNOS purification protocol. This work was supported by NIH (DK19038 (HBG); GM070868 (HBG); GM068461 (JRW)), by the Fannie and John Hertz Foundation (ARD), the Ellison Medical Foundation (Senior Scholar Award in Aging to HBG), a NSF graduate research fellowship (CAW), and the Arnold and Mabel Beckman Foundation.

References

1. Griffith OW, Stuehr DJ. Annu Rev Physiol 1995;57:707–736. [PubMed: 7539994]
2. Groves JT, Wang CC-Y. Curr Opin Chem Biol 2000;4:687–695. [PubMed: 11102875]
3. Davydov R, Ledbetter-Rogers A, Martásek P, Larukhin M, Sono M, Dawson JH, Masters BSS, Hoffman BM. Biochemistry 2002;41:10375–10381. [PubMed: 12173923]
4. Zhu Y, Silverman RB. Biochemistry 2008;47:2231–2243. [PubMed: 18237198]
5. Hurshman AR, Krebs C, Edmondson DE, Huynh BH, Marletta MA. Biochemistry 1999;38:15689–15696. [PubMed: 10625434]
6. Wei C-C, Wang Z-Q, Tejero J, Yang Y-P, Hemann C, Hille R, Stuehr DJ. J Biol Chem 2008;283:11734–11742. [PubMed: 18283102]
7. Robinet JJ, Cho K-B, Gauld JW. J Am Chem Soc 2008;130:3328–3334. [PubMed: 18293966]
8. Stuehr DJ, Santolini J, Wang Z-Q, Wei C-C, Adak S. J Biol Chem 2004;279:36167–36170. [PubMed: 15133020]
9. Tejero J, Biswas A, Wang Z-Q, Page RC, Haque MM, Hemann C, Zweier JL, Misra S, Stuehr DJ. J Biol Chem 2008;283:33498–33507. [PubMed: 18815130]
10. Wilker JJ, Dmochowski IJ, Dawson JH, Winkler JR, Gray HB. Angew Chem Int Edit 1999;38:89–92.
11. Dunn AR, Dmochowski IJ, Winkler JR, Gray HB. J Am Chem Soc 2003;125:12450–12456. [PubMed: 14531688]
12. Dmochowski IJ, Dunn AR, Wilker JJ, Crane BR, Green MT, Dawson JH, Sligar SG, Winkler JR, Gray HB. Method Enzymol 2002;357:120–133.

13. Belliston-Bittner W, Dunn AR, Nguyen YHL, Stuehr DJ, Winkler JR, Gray HB. J Am Chem Soc 2005;127:15907–15915. [PubMed: 16277534]
14. Nguyen YHL, Winkler JR, Gray HB. J Phys Chem B 2007;111:6628–6633. [PubMed: 17536854]
15. Beaumont E, Lambry JC, Gautier C, Robin AC, Gmouh S, Berka V, Tsai AL, Blanchard-Desce M, Slama-Schwok A. J Am Chem Soc 2007;129:2178–2186. [PubMed: 17263536]
16. Whited CA, Belliston-Bittner W, Dunn AR, Winkler JR, Gray HB. J Porphyrins Phthalocyanines 2008;12:971–978.
17. Dunn AR, Belliston-Bittner W, Winkler JR, Getzoff ED, Stuehr DJ, Gray HB. J Am Chem Soc 2005;127:5169–5173. [PubMed: 15810851]
18. Dunn, AR. Sensitizer-Linked Substrates as Probes of Heme Enzyme Structure and Catalysis [Ph D.]. Pasadena: California Institute of Technology; 2003.
19. Dmochowski, IJ. Probing Cytochrome P450 with Sensitizer-Linked Substrates [Ph.D.]. Pasadena: California Institute of Technology; 2000.
20. Hurshman AR, Marletta MA. Biochemistry 2002;41:3439–3456. [PubMed: 11876653]
21. Wang JL, Rousseau DL, Abusoud HM, Stuehr DJ. P Natl Acad Sci USA 1994;91:10512–10516.
22. Hurshman AR, Marletta MA. Biochemistry 1995;34:5627–5634. [PubMed: 7537092]
23. Abu-Soud HM, Wu C, Ghosh DK, Stuehr DJ. Biochemistry 1998;37:3777–3786. [PubMed: 9521697]
24. Low DW, Winkler JR, Gray HB. J Am Chem Soc 1996;118:117–120.
25. Kuciauskas D, Freund MS, Gray HB, Winkler JR, Lewis NS. J Phys Chem B 2001;105:392–403.
26. Dmochowski IJ, Winkler JR, Gray HB. J Inorg Biochem 2000;81:221–228. [PubMed: 11051567]
27. Garcin ED, Bruns CM, Lloyd SJ, Hosfield DJ, Tiso M, Gachhui R, Stuehr DJ, Tainer JA, Getzoff ED. J Biol Chem 2004;279:37918–37927. [PubMed: 15208315]
28. Chang I-J, Gray HB, Winkler JR. J Am Chem Soc 1991;113:7056–7057.
29. Rao PS, Hayon E. J Phys Chem 1975;79:1063–1066.
30. Fujita S, Steenken S. J Am Chem Soc 1981;103:2540–2545.
31. Hobel B, von Sonntag C. Journal of the Chemical Society, Perkin Transactions 1998;2:509–513.
32. Schweizer M, Richter C. Biochem Bioph Res Co 1994;204:169–175.
33. Devoe IW, Gilchrist JE. J Bacteriol 1976;128:144–148. [PubMed: 824266]
34. Marchal S, Gorren ACF, Sorlie M, Andersson KK, Mayer B, Lange R. J Biol Chem 2004;279:19824–19831. [PubMed: 15004019]
35. Roman LJ, Masters BSS. J Biol Chem 2006;281:23111–23118. [PubMed: 16782703]
36. Migita CT, Salerno JC, Masters BSS, Martasek P, McMillan K, Ikeda-Saito M. Biochemistry 1997;36:10987–10992. [PubMed: 9283090]
37. Huang L, Abu-Soud HM, Hille R, Stuehr DJ. Biochemistry 1999;38:1912–1920. [PubMed: 10026272]
38. de Rosny E, de Groot A, Jullian-Binard C, Borel F, Suarez C, Le Pape L, Fontecilla-Camps JC, Jouve HlnM. Biochemistry 2008;47:13252–13260. [PubMed: 19086271]
39. Raphael AL, Gray HB. J Am Chem Soc 1991;113:1038–1040.
40. Matsui T, Nagano S, Ishimori K, Watanabe Y, Morishima I. Biochemistry 1996;35:13118–13124. [PubMed: 8855949]
41. Denisov IG, Makris TM, Sligar SG. Method Enzymol 2002;357:103–115.

Abbreviations

tmRu-F_9bp
: $[(4,4',5,5'\text{-tetramethylbipyridine})_2Ru(F_9bp)]^{2+}$

F_9bp
: (4-methyl-4'-methylperfluorobiphenylbipyridine)

NO
: nitric oxide

NOS
nitric oxide synthase

iNOSoxy
isolated oxygenase domain of murine inducible NOS

NHA
N^G-hydroxy-L-arginine

ET
electron transfer

BH_4 / pterin
tetrahydrobiopterin

TMPD
tetramethylphenylenediamine

Asc
ascorbate

Q
quencher

B-PER
protein extraction reagent B (Pierce)

P_i
phosphate, PO_4^{2-}

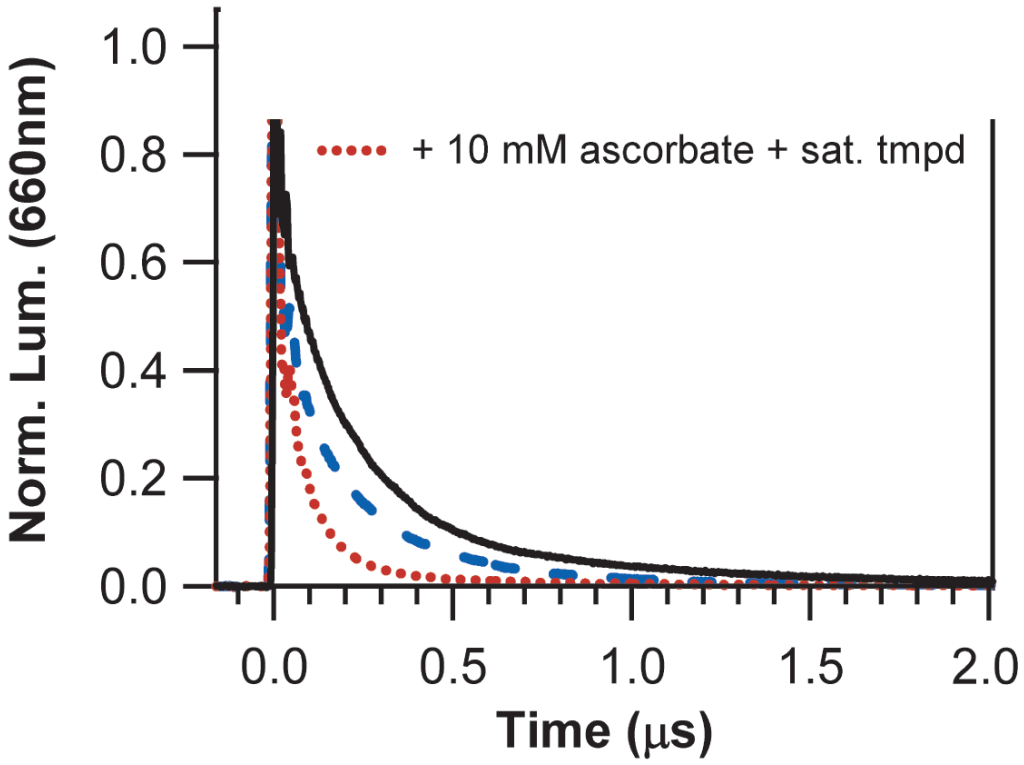

Figure 1.
Luminescence decay of 6.2 μM tmRu-F_9bp bound to equimolar Im-iNOSoxy in the absence of quenchers (black line) and in the presence of 10 mM Asc (blue dashes) or 10 mM Asc and saturated TMPD (red dots). λ_{ex} = 480 nm and λ_{obs} = 660 nm.

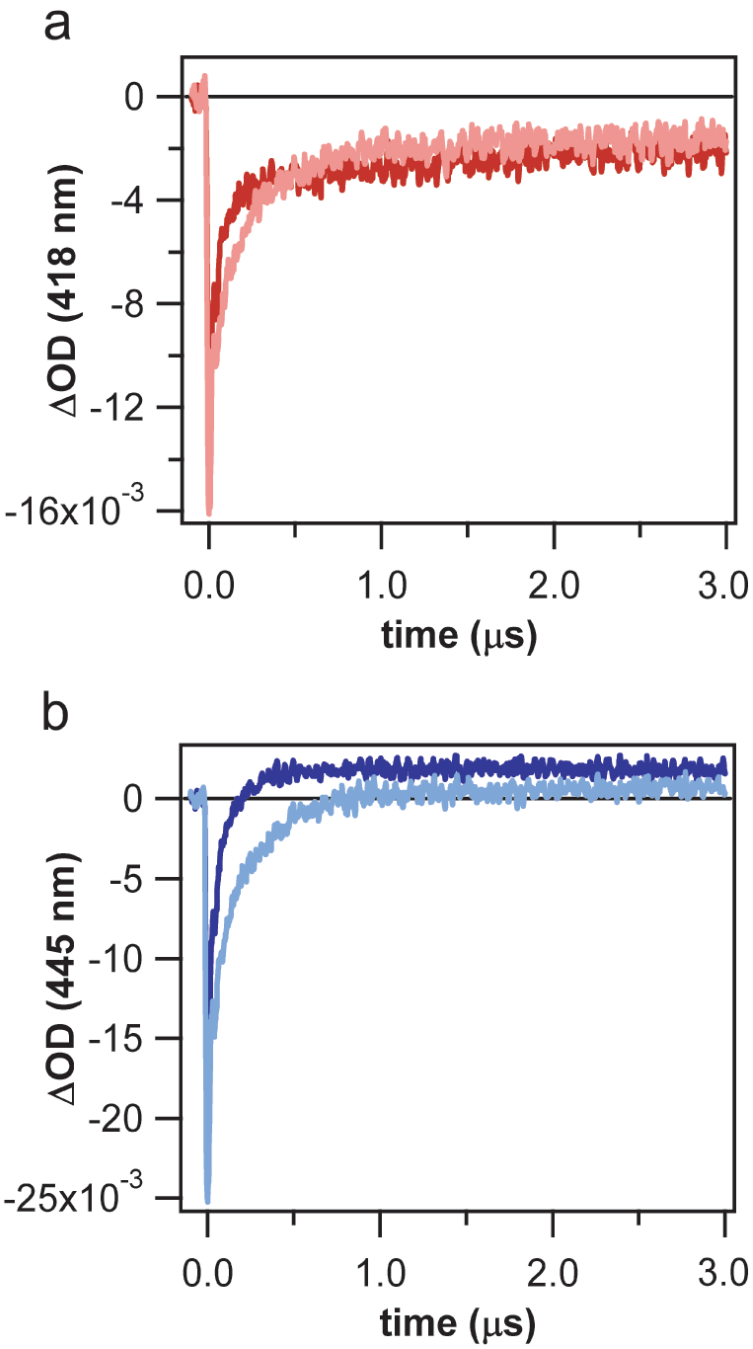

Figure 2.

Transient absorbance of 1:1 mixtures of tmRu-F_9bp and Im-iNOSoxy (6.2 μM) in the presence of 10 mM Asc with (darker traces) and without (lighter traces) saturated TMPD. λ_{ex} = 480 nm. a) λ_{obs} = 418 nm. b) λ_{obs} = 445 nm. The addition of TMPD increases the yield of reduced heme.

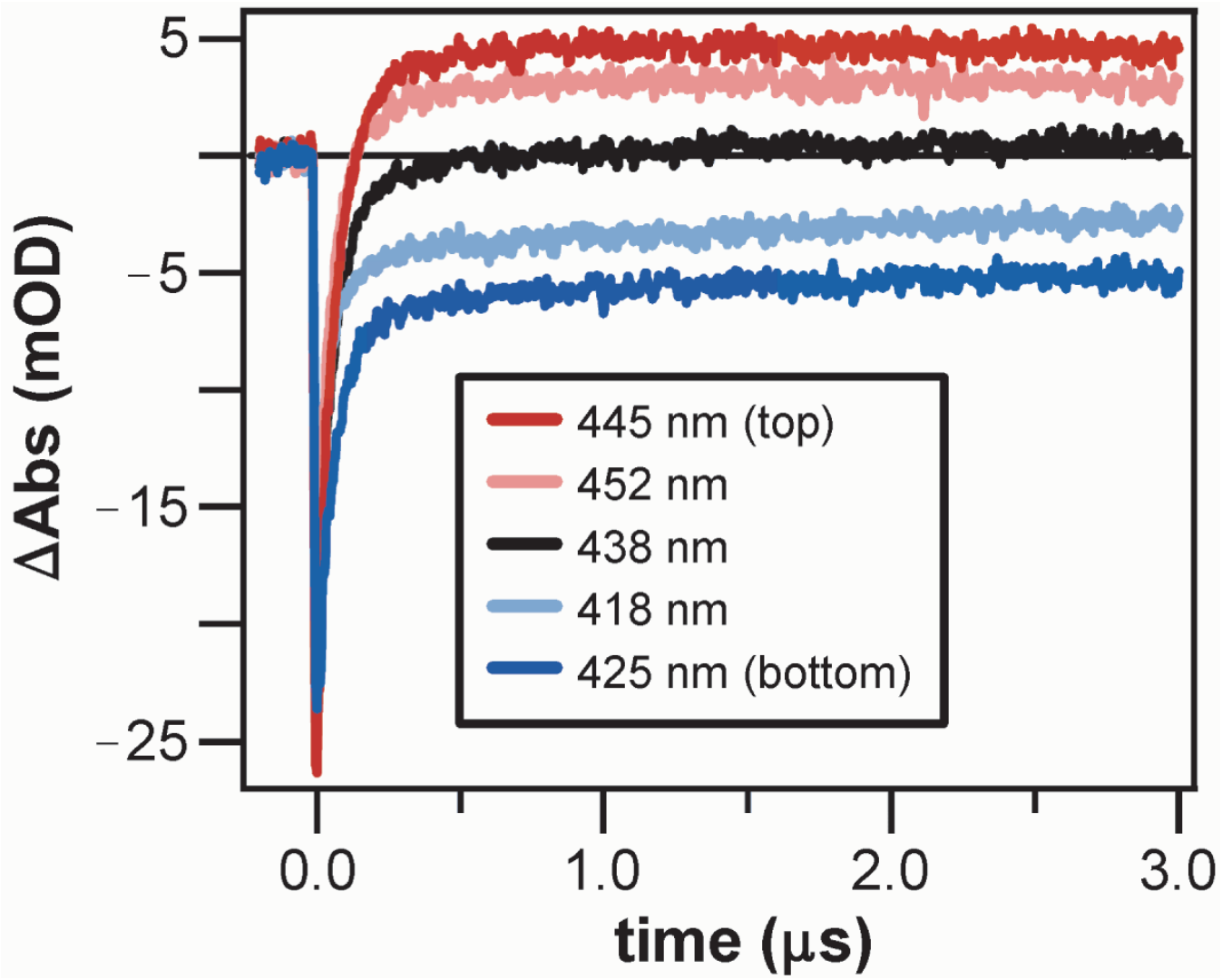

Figure 3.
Transient absorbance of quenched Im-iNOSoxy bound to 1 equivalent of tmRu-F_9bp (11 μM with 10 mM Asc and saturated TMPD). λ_{ex} = 480 nm.

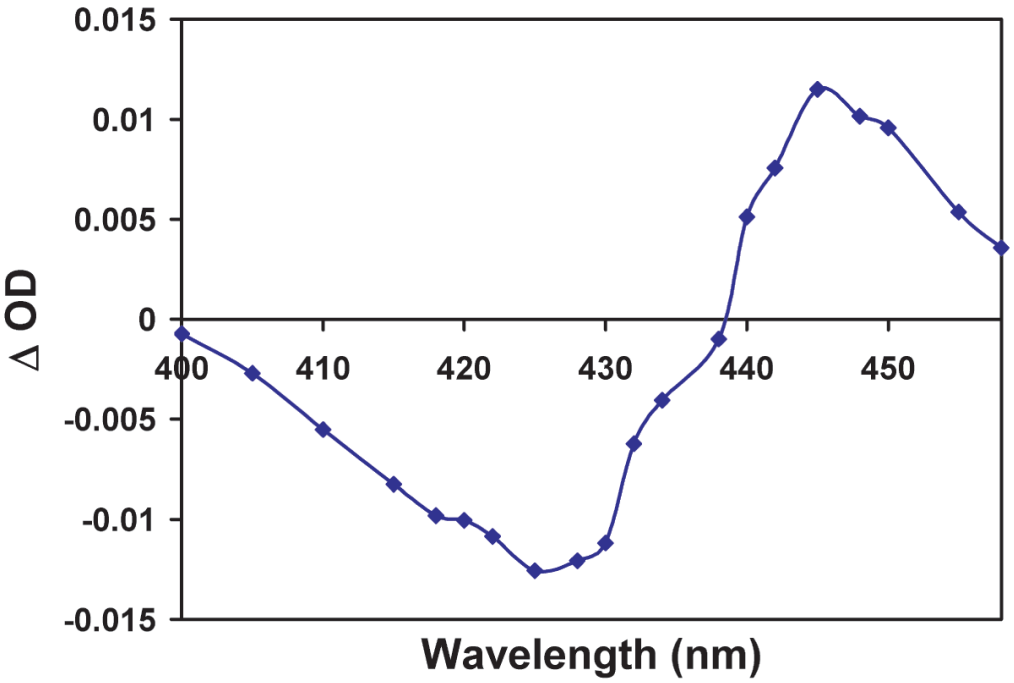

Figure 4.

Transient absorbance of a 1:1 mixture of Im-iNOSoxy and tmRu-F_9bp (22 μM with 10 mM Asc and saturated TMPD) showing a characteristic Fe(III/II) difference spectrum. Individual points were taken from single wavelength transient absorbance traces at 2 μs after excitation at 480 nm.

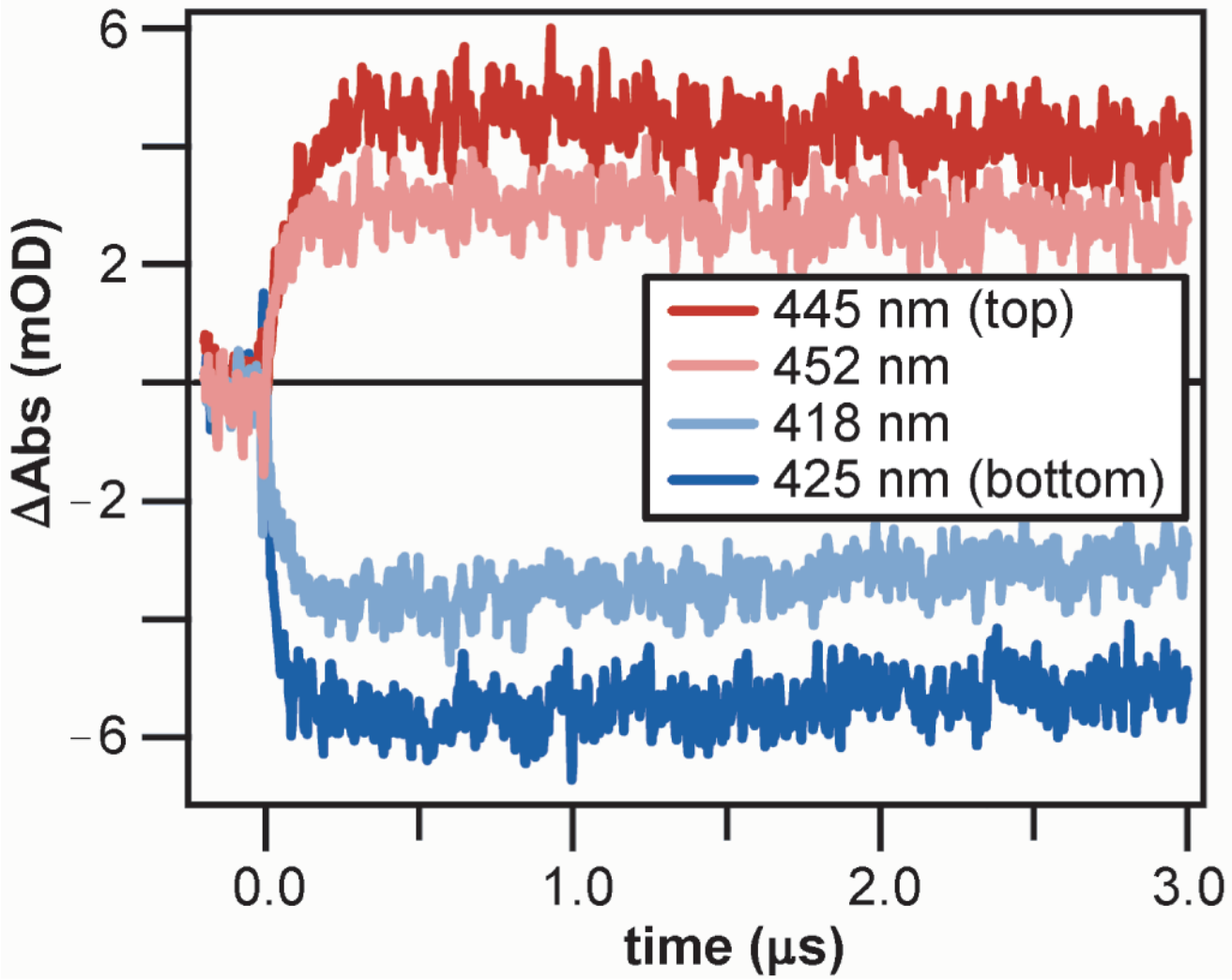

Figure 5.
Transient absorbance of Im-iNOSoxy bound to 1 equivalent of tmRu-F_9bp (11 μM with 10 mM Asc and saturated TMPD) corrected for absorbance due to $*Ru^{II}$: k_{ET} = 2(1)×10^7 s^{-1}; λ_{ex} = 480 nm.

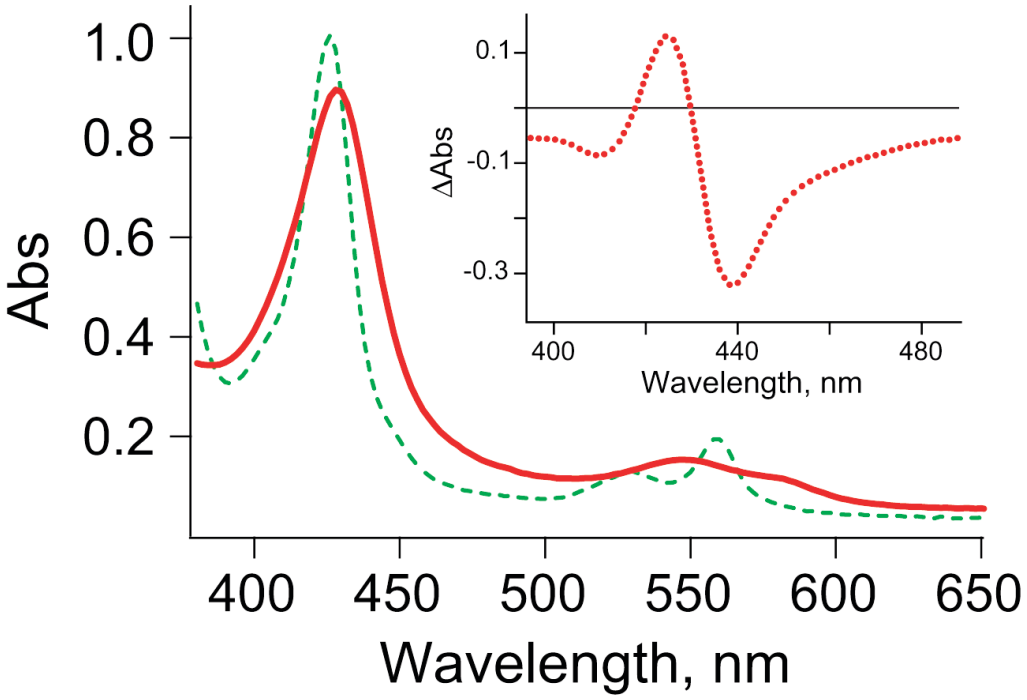

Figure 6.
Steady-state spectra of ferric-imidazole (red solid line) and the reduced species (green dashed line). Inset: The difference spectrum generated upon reduction (red dotted line).

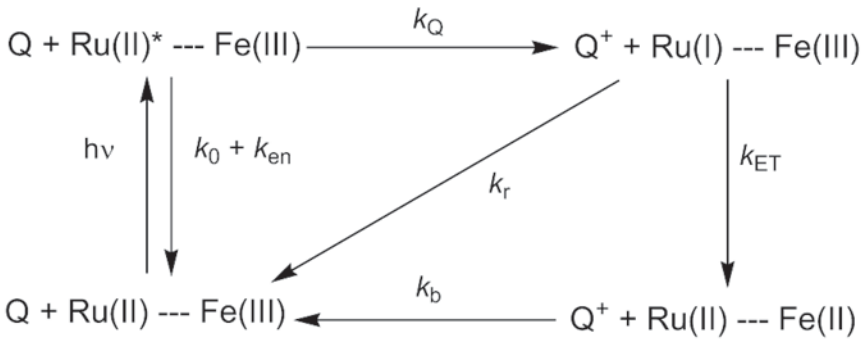

Scheme 1.

Representation of the reversible flash/quench experiment employed in this work. For simplicity, TMPD and ascorbate are represented together as Q. In a successful flash/quench experiment, quenching must compete with intrinsic relaxation (k_0) and energy transfer (k_{en}) for depletion of the Ru^{II} excited state ($k_Q[Q] \geq k_0 + k_{en}$); and electron transfer (k_{ET}) must be faster than recombination between oxidized quencher and reduced sensitizer ($t½ = 1/k_r[Ru^I]_0$).

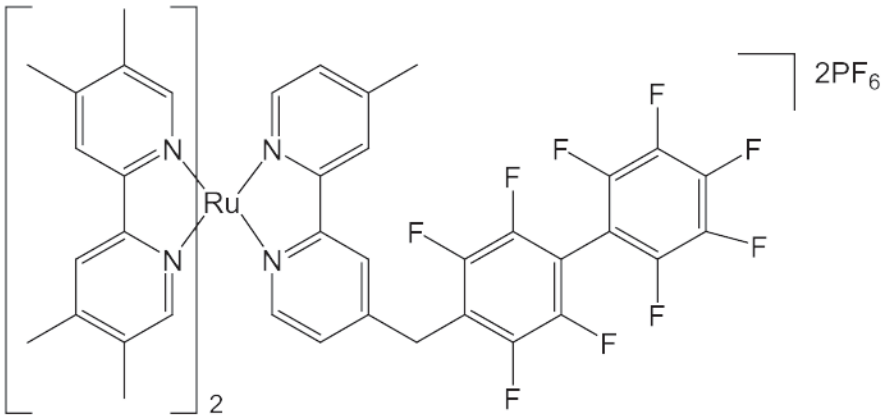

Chart 1.
tmRu-F_9bp.